Available online at www.sciencedirect.com
SCIENCE DIRECT®
Journal of Sound and Vibration 287 (2005) 481–503
JOURNAL OF SOUND AND VIBRATION
www.elsevier.com/locate/jsvi

Active structural acoustics control of beams using active constrained layer damping through loss factor maximization

Joshua T. Lee*

Mechanical and Aerospace Engineering Department, University of California, Los Angeles, CA 90095, USA

Received 4 May 2004; received in revised form 19 October 2004; accepted 11 November 2004
Available online 12 January 2005

Abstract

Vibration and acoustic control of beams with classical boundary conditions using active constrained layer damping is presented. The control input that maximizes the loss factor of the active constrained layer damping is determined through taking the first variation of the loss factor with respect to the control input. Although the loss factor is a positive definite quantity, the first variation yields control input that maximizes the factor. The resulting control input significantly reduces the vibration and acoustic response of the beams at their resonant frequencies.

1. Introduction

There are several methods to control the vibration of structures and their induced noise. One of the widely used methods in tackling this problem are applying passive damping treatments. Of all the treatments, a popular choice is constrained layer viscoelastic damping. It is quite easy to apply and generally effective in reducing both vibration and structure-borne noise in the high-frequency range. There have been extensive researches done on mechanics and performance optimizations of the passive constrained layer treatments. Lall, Mead, Kung, and various researchers applied energy-related approaches to generate governing equations with associated boundary conditions [1–6]. Usually, this approach works well for the damping treatment with uniform coverage over a

*Corresponding author. Boeing Phantom Works, Mail Code H013-B308, 5301 Bolsa Avenue, Huntington Beach, CA 92647, USA. Tel.: +1 714 896 1344; fax: +1 714 896 1559.
E-mail address: joshua.t.lee@boeing.com (J.T. Lee).

0022-460X/$ - see front matter © 2004 Elsevier Ltd. All rights reserved.
doi:10.1016/j.jsv.2004.11.006

Nomenclature

$A11$ extensional stiffness coefficient
$\overline{A11}$ nondimensionalized extensional stiffness coefficient ($= A11a^2/D11_b$)
$\overline{\mathbf{C}}^k$ nondimensionalized rigid modal amplitude vector of the longitudinal modes of the kth constrained layer
$D11$ flexural stiffness coefficient
$\overline{D11}$ nondimensionalized flexural stiffness coefficient ($= D11/D11_b$)
E applied electric field ($= V/h_c$)
G shear modulus of viscoelastic material
$\overline{G}$ nondimensionalized shear modulus of viscoelastic material ($= Ga^3/D11_b$)
H Heaviside function that describes the location of the active constrained layer
$[\mathbf{K}]$ stiffness matrix or stiffness matrix coefficient terms
L Lagrangian
$[\mathbf{M}]$ mass matrix or mass matrix coefficient terms
P radiated sound pressure
$Q(k,n,\xi)$ longitudinal mode shapes of the constrained layer in ξ-direction ($k = k$th ACLD, $n =$ mode number)
$Q11_c$ Young's modulus of the constrained layer
P_o external pressure load
$\overline{P_o}$ nondimensionalized external pressure load ($= P_o(a^4/h_bD11_b)$)
T kinetic energy
U potential energy
$\overline{\mathbf{U}}^k$ nondimensionalized modal amplitude vector of the longitudinal modes of the kth constrained layer
V applied voltage
$\overline{\mathbf{W}}$ nondimensionalized modal amplitude vector of the flexural modes of the beam
$\overline{\mathbf{W}_{\mathrm{EX}}}$ nondimensionalized work done by applied loads
$X(m,\xi)$ flexural mode shapes of the beam in ξ-direction ($m =$ mode shape)
$Y(\eta)$ structural mode shapes in η-direction
a length of the beam
b width of the beam
c speed of sound
d_{31} piezoelectric constant for the constrained layer
f external point load
$\overline{f}$ nondimensionalized magnitude of an external point load ($= f(a^3/h_bD11_b)$)
h thickness
k acoustic wavenumber
m mass/length
$\overline{m}$ normalized mass/length ($= m(a^4/D11_b)$)
t time
u longitudinal displacement field
$\overline{u}_b$ normalized longitudinal displacement field ($= u/h_b$)
w transverse displacement field
$\overline{w}$ normalized transverse displacement field ($= w/h_b$)
Π average radiated sound power
δ Dirac delta function indicating location of an external point load
$\overline{\varepsilon}^k_{\mathrm{cpe}}$ normalized piezoelectric strain ($= (a/h_b)d_{31}E$)
γ shear strain
ω circular frequency
ξ nondimensional variable in x-direction ($\xi = x/a$)
η nondimensional variable in y-direction ($\eta = y/b$)

Subscripts

b beam
c constrained layer
con control
d dissipated
Ex external
Pt.Force point force
v viscoelastic layer
uu $\overline{U}^k_c$ terms coupling with $\overline{U}^k_c$ terms
uw $\overline{U}^k_c$ terms coupling with $\overline{W}$ terms
uc $\overline{U}^k_c$ terms coupling with $\overline{C}^k$ terms
wu $\overline{W}$ terms coupling with $\overline{U}^k_c$ terms
ww $\overline{W}$ terms coupling with $\overline{W}$ terms
wc $\overline{W}$ terms coupling with $\overline{C}^k$ terms
cu $\overline{C}^k$ terms coupling with $\overline{U}^k_c$ terms
cw $\overline{C}^k$ terms coupling with $\overline{W}$ terms
cc $\overline{C}^k$ terms coupling with $\overline{C}^k$ terms

Superscript

k kth ACLD

structure. For discrete damping treatment coverage cases, Lagrange's equation and finite element modeling are the preferred approaches [7–11]. Many of the performance improvement studies inquire various design parameters, such as length optimization and optimal locations [2,9,10].

A recently introduced damping concept to improve the performance of passive constrained layer treatments is active constrained layer damping (ACLD). The ACLD approach consists of a viscoelastic damping layer combined with a constrained layer that is made of a smart material, like PZT. Fig. 1 depicts a general scheme of a beam with an ACLD. By integrating the ACLD with an appropriate combination of sensors and controllers, a higher reduction in vibration and noise can be accomplished.

There are numerous studies being done on the ACLD for structural control. Baz [12–15] has investigated the performance of the ACLD using the boundary controller. The boundary controller depends on knowing the strain information of the active constrained layer. Therefore, either there must be a sensor attached to the constrained layer, or it must be a self-sensing actuator [15,16]. There are many studies analyzing the performance of various control schemes, including H_∞ and LQG [17–19]. Also, there are numerous parametric studies conducted to optimize the performance of the ACLD, focusing on identifying the optimal performance zone [16,20,21]. Baz [13,14] and Shen [16] have investigated the energy dissipating mechanism of the ACLD. A rate feedback mechanism is utilized as the active energy dissipative mechanism.

To enhance the performance of the ACLD, a number of variations of the ACLD are investigated. Liao et al. [22–24] proposed the ACLD with edge spring mechanisms attached at the ends of the active constrained layer. This increases force transmission by the constrained layer to the host structure. Another variation proposed by Rongong et al. [25] uses a passive constrained layer damping configuration with a layered actuator on top of the constrained layer. Also, an integrated system proposed by Lam et al. [26] consists of passive constrained layer viscoelastic damping treatments and conventional piezoceramic actuators.

While the researchers have shown that the active constrained layer damping is an effective means to control vibration, they have not quantitatively investigated the contribution of the energy dissipation mechanism in reducing vibration, especially for low-frequency resonant responses. Consequently, a majority of the previous researches utilized the conventional means, which is using the ACLD primarily as a control force generator. In doing so, the damping mechanism takes a secondary role in controlling the vibration.

The proposed approach is a method to compute the control input that directly takes advantage of the damping mechanism. The control input is computed through maximizing the overall loss factor of the structural system with the ACLD [30]. This paper is divided into 3 sections. First, the mathematical modeling of the ACLD and the loss factor maximization scheme are illustrated. Second, the mathematical model of the ACLD is validated using an experimental result. Third, the performance of the loss factor maximization scheme in reducing structural response is discussed in detail.

2. Theory of active constrained layer damping

The structural model of a thin beam with the ACLD makes the following assumptions:

1. Linear classical beam theory is applicable. Therefore, flexural displacement and slope are going to be same throughout the thickness of the ACLD. All displacements are assumed small.

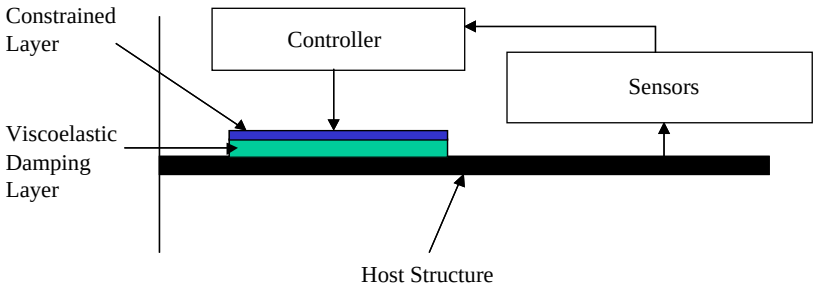

Fig. 1. A general layout of a beam with active constrained layer damping (ACLD).

2. Moduli of the viscoelastic layer are negligible compared to either the host beam or the constrained layer. Therefore, extensional and bending strain energies of the viscoelastic layer are neglected. The shear effect is assumed the most dominant feature in the layer.
3. Perfect bonding exists between the layers. Therefore, there is no slip condition at the interfaces.
4. Adhesive effects are ignored.
5. The damping layer is linear viscoelastic.

2.1. The kinematics of the viscoelastic damping layer

The primary damping mechanism of the viscoelastic layer comes from its induced shear strain by the host structure and the constrained layer. The expression of the induced shear strain at the kth viscoelastic layer as shown in Fig. 2 is

$$\gamma^k = \frac{u_c^k - u_b}{h_v} + \alpha \frac{\partial w}{\partial x}, \tag{1}$$

where

$$\alpha = 1 + \frac{h_b + h_c}{2h_v}. \tag{2}$$

The shear strain is assumed uniform throughout the thickness of the viscoelastic damping layer. The detailed derivation of Eqs. (1) and (2) is covered by Lall et al. [7,8].

2.2. Governing equations of a beam with the ACLD

To derive the system of governing equations, Lagrange's equation of motion is used. It expresses the equations of motion in terms of generalized coordinates and is obtained using the internal structural energy components and the work done by external forces. The following equations represent the nondimensionalized strain and kinetic energies per unit width of a beam with the ACLD:

$$\overline{U}_{\mathrm{Tot}} = \overline{U}_b + \overline{U}_c + \overline{U}_v, \quad \overline{T}_{\mathrm{Tot}} = \overline{T}_b + \overline{T}_c + \overline{T}_v, \tag{3,4}$$

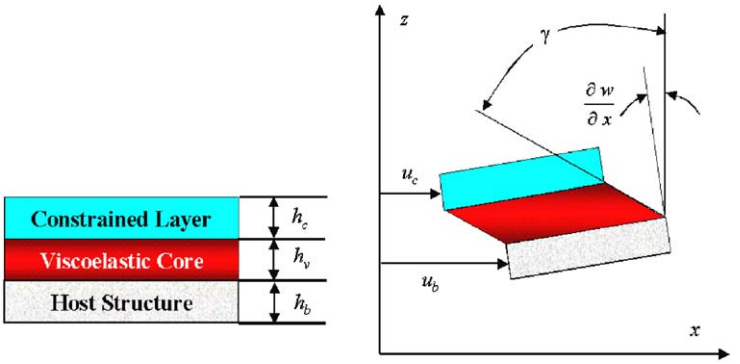

Fig. 2. Deformation diagram of a viscoelastic layer damping system.

where

$$\overline{U}_b = \frac{1}{2}\int_0^1 \overline{A11}_b \left(\frac{\partial \overline{u}_b}{\partial \xi}\right)^2 \mathrm{d}\xi + \frac{1}{2}\int_0^1 \overline{D11}_b \left(\frac{\partial^2 \overline{w}}{\partial \xi^2}\right)^2 \mathrm{d}\xi, \tag{5a}$$

$$\overline{U}_c = \frac{1}{2}\sum_k \int_0^1 (H(\xi-\xi_1^k) - H(\xi-\xi_2^k))\overline{A11}_c \left(\frac{\partial \overline{u}_c^k}{\partial \xi} - \overline{\varepsilon}_{\mathrm{cpe}}^k\right)^2 \mathrm{d}\xi,$$
$$+\frac{1}{2}\sum_k \int_0^1 (H(\xi-\xi_1^k) - H(\xi-\xi_2^k))\overline{D11}_c \left(\frac{\partial^2 \overline{w}}{\partial \xi^2}\right)^2 \mathrm{d}\xi, \tag{5b}$$

$$\overline{U}_v = \frac{1}{2}\overline{G}\sum_k \int_0^1 (H(\xi-\xi_1^k) - H(\xi-\xi_2^k)) \begin{pmatrix} \frac{a}{h_v}\left(\overline{u}_c^k - \overline{u}_b\right)^2 \\ +2\alpha\left(\overline{u}_c^k - \overline{u}_b\right)\frac{\partial \overline{w}}{\partial \xi} \\ +\frac{h_v}{a}\alpha^2\left(\frac{\partial \overline{w}}{\partial \xi}\right)^2 \end{pmatrix} \mathrm{d}\xi, \tag{5c}$$

$$\overline{T}_b = \frac{1}{2}\int_0^1 \overline{m}_b \left(\frac{\partial \overline{u}_b}{\partial t}\right)^2 \mathrm{d}\xi + \frac{1}{2}\int_0^1 \overline{m}_b \left(\frac{\partial \overline{w}}{\partial t}\right)^2 \mathrm{d}\xi, \tag{6a}$$

$$\overline{T}_c = \frac{1}{2}\sum_k \int_0^1 (H(\xi-\xi_1^k) - (\xi-\xi_2^k))\overline{m}_c \left(\frac{\partial \overline{u}_c^k}{\partial t}\right)^2 \mathrm{d}\xi,$$
$$+\frac{1}{2}\sum_k \int_0^1 (H(\xi-\xi_1^k) - (\xi-\xi_2^k))\overline{m}_c \left(\frac{\partial \overline{w}}{\partial t}\right)^2 \mathrm{d}\xi, \tag{6b}$$

$$\overline{T}_v = \frac{1}{2}\sum_k \int_0^1 (H(\xi-\xi_1^k) - (\xi-\xi_2^k))\overline{m}_v \left(\frac{\partial \overline{w}}{\partial t}\right)^2 \mathrm{d}\xi. \tag{6c}$$

The dimensioned energy expressions can be found in many Refs. [1,3,4,7–9]. The energy expressions are normalized with the expression $a^3/(D11_b h_b^2)$ and the displacement fields with the thickness of the beam, h_b. The Heaviside functions indicate the segment of the host beam where the viscoelastic damping layers are placed.

A general normalized expression of work done by external loads is

$$\overline{W_{\mathrm{EXext}}} = \int_0^1 \left(\overline{P}_o(\xi,\omega,t) + \sum_q \overline{f}_q \delta(\xi - \xi_{\mathrm{pt.force}_q}) \right) \overline{w}(\xi,\omega,t)\,\mathrm{d}\xi. \tag{7}$$

As Eq. (5b) indicates, there is no work being done directly on the host beam by the active constrained layer. In fact, the lack of this feature has caused many researchers to introduce a number of auxiliary mechanical means to increase transmissibility of the control force to the host structure [22–24].

The current model of a beam with the ACLD has 3 independent displacement fields: $\bar{u}_c^k$, $\bar{u}_b$, and $\bar{w}$. To reduce the number of independent fields from 3 to 2, the following static passive longitudinal force equilibrium relationship between the host beam and kth constrained layer is employed:

$$\overline{A11}_b \frac{\partial \overline{u}_b}{\partial \xi} + \overline{A11}_c \frac{\partial \overline{u}_c^k}{\partial \xi} = 0, \quad \overline{A11}_b \overline{u}_b + \overline{A11}_c \overline{u}_c^k = C'. \tag{8a,b}$$

The force component of the viscoelastic layer is absent because of the previous assumption of its negligible extensional stiffness. Without a loss in generality,

$$\overline{u}_b = -\left(\frac{\overline{A11}_c}{\overline{A11}_b} \right) \overline{u}_c^k + \overline{C}_o = -c1(\overline{u}_c^k + \overline{C}). \tag{9}$$

The independent displacement fields are expressed as linear combinations of assumed mode shapes. Therefore, in terms of assumed mode shapes,

$$\overline{u}_c^k(\xi,\omega,t) = \mathrm{e}^{\mathrm{j}\omega t} \left(\sum_n^{N3} \overline{U}_c^k Q(k,n,\xi) + \overline{C}^k \right) = \overline{\mathbf{U}}_c^{k^{\mathrm{T}}} \mathbf{Q} + \overline{\mathbf{C}}^k, \tag{10a}$$

$$\overline{u}_b = -c1\overline{u}_c^k, \quad \overline{w}(\xi,\omega,t) = \mathrm{e}^{\mathrm{j}\omega t} \sum_{m=1}^{N5} \overline{W}_m X(m,\xi) = \overline{\mathbf{W}}^{\mathrm{T}} \mathbf{X}. \tag{10b,c}$$

Details of the mode shapes are listed in Appendix A. With Eqs. (10), the longitudinal displacement field of the beam becomes a function of the equivalent field of the kth constrained layer. A constant $\overline{C}^k$ is introduced in the longitudinal displacement field of the constrained layer to represent its rigid motion at the ends. Because it is an arbitrary modal amplitude, $\overline{C}^k$ can represent $\overline{C}$ of Eq. (9) without a loss of generality.

The assumed shape functions must satisfy admissible boundary conditions. For $\overline{u}_c^k$, because of its unconstrained end conditions, it must satisfy the following boundary conditions:

$$\overline{u}_c^k(\xi = 0, 1) \neq 0, \quad \frac{\partial \overline{u}_c^k(\xi = 0, 1)}{\partial \xi} = d_{31_c} E_c^k. \tag{11a,b}$$

Notice that Eq. (11b) reverts to the passive constrained layer boundary condition if the controller becomes inactive. For the beam transverse displacement fields, there are well-defined shape functions for a number of classical boundary conditions. In this paper, beams with the 3 classical boundary conditions are considered; simply supported, fully clamped, and cantilevered. The longitudinal functions are previously reported by Lall et al. [7,8] and the flexural mode shapes by Leissa [27].

With the selected shape functions, the governing system equations can be generated. Let L be the Lagrangian

$$L = \overline{T}_{\text{Tot}} - \overline{U}_{\text{Tot}}. \tag{12}$$

Then, applying Lagrange's equations,

$$\frac{\mathrm{d}}{\mathrm{d}t}\left(\frac{\partial L}{\partial \dot{\overline{\mathbf{U}}}_c^k}\right) - \frac{\partial L}{\partial \overline{\mathbf{U}}_c^k} = \frac{\partial \overline{W_{\text{EXExt}}}}{\partial \overline{\mathbf{U}}_c^k}, \tag{13a}$$

$$\frac{\mathrm{d}}{\mathrm{d}t}\left(\frac{\partial L}{\partial \dot{\overline{\mathbf{W}}}}\right) - \frac{\partial L}{\partial \overline{\mathbf{W}}} = \frac{\partial \overline{W_{\text{EXExt}}}}{\partial \overline{\mathbf{W}}}, \tag{13b}$$

$$\frac{\mathrm{d}}{\mathrm{d}t}\left(\frac{\partial L}{\partial \dot{\overline{\mathbf{C}}}^k}\right) - \frac{\partial L}{\partial \overline{\mathbf{C}}^k} = \frac{\partial \overline{W_{\text{EXExt}}}}{\partial \overline{\mathbf{C}}^k}, \tag{13c}$$

the system of governing equations in the following general format can be generated:

$$\left[-\omega^2 \begin{bmatrix} \mathbf{M}_{uu} & \mathbf{M}_{uw} & \mathbf{M}_{uc} \\ \mathbf{M}_{wu} & \mathbf{M}_{ww} & \mathbf{M}_{wc} \\ \mathbf{M}_{cu} & \mathbf{M}_{cw} & \mathbf{M}_{cc} \end{bmatrix} + \begin{bmatrix} \mathbf{K}_{uu} & \mathbf{K}_{uw} & \mathbf{K}_{uc} \\ \mathbf{K}_{wu} & \mathbf{K}_{ww} & \mathbf{K}_{wc} \\ \mathbf{K}_{cu} & \mathbf{K}_{cw} & \mathbf{K}_{cc} \end{bmatrix} + \mathrm{j} \begin{bmatrix} \mathbf{K}''_{uu} & \mathbf{K}''_{uw} & \mathbf{K}''_{uc} \\ \mathbf{K}''_{wu} & \mathbf{K}''_{ww} & \mathbf{K}''_{wc} \\ \mathbf{K}''_{cu} & \mathbf{K}''_{cw} & \mathbf{K}''_{cc} \end{bmatrix}\right] \begin{Bmatrix} \overline{\mathbf{U}}_c^k \\ \overline{\mathbf{W}} \\ \overline{\mathbf{C}}^k \end{Bmatrix} = \begin{Bmatrix} \mathbf{0} \\ \overline{\mathbf{f}}_{\text{ext}} \\ \mathbf{0} \end{Bmatrix} + \begin{Bmatrix} \overline{\mathbf{f}}_{\text{con}} \\ \mathbf{0} \\ \mathbf{0} \end{Bmatrix}. \tag{14}$$

A general expression of the resulting modal amplitude vector is

$$\begin{Bmatrix} \overline{\mathbf{U}}_c^k \\ \overline{\mathbf{W}} \\ \overline{\mathbf{C}}^k \end{Bmatrix} = \begin{Bmatrix} \mathbf{Ex}_{Uc}^k \\ \mathbf{Ex}_w \\ \mathbf{Ex}_C^k \end{Bmatrix} + \begin{bmatrix} \mathbf{Fc}_{Uc}^k \\ \mathbf{Fc}_W \\ \mathbf{Fc}_C^k \end{bmatrix} \mathbf{V}_{\text{con}}. \tag{15}$$

The vector $\{\mathbf{Ex}_{Uc}^{k}\,\mathbf{Ex}_{w}\,\mathbf{Ex}_{C}^{k}\}^{\mathrm{T}}$ is the modal amplitude due to the external forces and the matrix $[\mathbf{Fc}_{Uc}^{k^{\mathrm{T}}}\,\mathbf{Fc}_{W}^{\mathrm{T}}\,\mathbf{Fc}_{C}^{k^{\mathrm{T}}}]^{\mathrm{T}}$ due to the control input.

2.3. Maximization of the loss factor

There are in general two ways to use the ACLD to control vibration; a conventional actuator and an energy dissipation enhancer. The key disadvantage of using the ACLD as an actuator is that the transmissibility of the control force onto the host structure is significantly degraded due to the viscoelastic damping layer [21]. The ACLD can be used more effectively in controlling the structural response if it is employed to enhance the energy dissipating capability.

According to Lee and Plunkett [2], the energy dissipated per cycle per unit length per width with a constrained layer damping treatment is

$$d(\Delta W_d) = \pi h_v \,\mathrm{Im}(G)\gamma^2 = \pi h_v G''\gamma^2. \tag{16}$$

Therefore, after applying the expression of the shear strain, an expression for a normalized dissipated energy per cycle by the kth ACLD that partially covers a beam from ξ_1^k to ξ_2^k per width is

$$\Delta\overline{W}_d^k = \pi\overline{G}'' \int_0^1 (H(\xi-\xi_1^k) - H(\xi-\xi_2^k)) \begin{bmatrix} \left(\dfrac{a}{h_v}\right)(1+c1)^2 \overline{u}_c^k \overline{u}_c^{k*} \\ +(1+c1)\alpha\left(\overline{u}_c^k \dfrac{\partial \overline{w}^*}{\partial\xi} + \overline{u}_c^{k*} \dfrac{\partial \overline{w}}{\partial\xi}\right) \\ +\left(\dfrac{h_v}{a}\right)\alpha^2 \dfrac{\partial \overline{w}}{\partial\xi}\dfrac{\partial \overline{w}^*}{\partial\xi} \end{bmatrix} \mathrm{d}\xi \tag{17}$$

After substituting the displacement field variables with the shape functions and performing the integration, Eq. (17) can be expressed in the general form

$$\Delta\overline{W}_d^k = \begin{Bmatrix} \overline{\mathbf{U}}_c^k \\ \overline{\mathbf{W}} \\ \overline{\mathbf{C}}^k \end{Bmatrix}^{\mathrm{H}} \begin{bmatrix} \mathbf{DE}_{11} & \mathbf{DE}_{12} & \mathbf{DE}_{13} \\ \mathbf{DE}_{21} & \mathbf{DE}_{22} & \mathbf{DE}_{23} \\ \mathbf{DE}_{31} & \mathbf{DE}_{32} & \mathbf{DE}_{33} \end{bmatrix} \begin{Bmatrix} \overline{\mathbf{U}}_c^k \\ \overline{\mathbf{W}} \\ \overline{\mathbf{C}}^k \end{Bmatrix}. \tag{18}$$

By applying the modal amplitude expressions of Eq. (15) and rearranging Eq. (18), the dissipated energy expression for kth ACLD takes the form

$$\begin{aligned} \Delta\overline{W}_d^k = {} & V_{\mathrm{con}}(k)^* \mathrm{DE}_Q(k) V_{\mathrm{con}}(k) + \mathrm{DE}_S(k) V_{\mathrm{con}}(k) \\ & + V_{\mathrm{con}}(k)^* \mathrm{DE}_T(k) + \mathrm{DE}_p(k). \end{aligned} \tag{19}$$

$\mathrm{DE}_Q(k)$ is a dissipated energy term due to purely active components. $\mathrm{DE}_S(k)$ and $\mathrm{DE}_T(k)$ are the coupled energy terms between the active and passive components. The dissipated energy due to the passive damping treatment is represented by $\mathrm{DE}_p(k)$. Because the expression is quadratic and positive definite, taking the first variation of the expression with respect to $V_{\mathrm{con}}(k)$ yields a control voltage that minimizes the dissipated energy, not a desirable strategy.

One convenient variable that shows a relative measurement of the dissipated energy is a loss factor. The loss factor is a ratio between a dissipated energy and a reference elastic strain energy

per cycle. The loss factor shown in Eq. (20) is a ratio between the dissipated energy of the kth ACLD and the bending strain energy of the host structure as the reference strain energy. The most commonly used strain energy expression in defining the loss factor is the total strain energy of the entire structural system. But, in this analysis, it is assumed that the strain energy of the host beam due to the flexural motion is the most critical component. Therefore,

$$\eta^k = \frac{\Delta \overline{W}_d^k}{2\pi \overline{U}_{\text{ref}}}, \quad \overline{U}_{\text{ref}} = \overline{U}_{\text{bending}} = \frac{1}{2}\overline{D11}_b \frac{\partial^2 \overline{w}^*}{\partial \xi^2} \frac{\partial^2 \overline{w}}{\partial \xi^2}. \tag{20}$$

The factor 2π in the denominator of the loss factor is present because the dissipative energy is computed per cycle. The detailed derivation of the loss factor expression can be found in a number of Refs. [2,5,6]. Similar to the dissipated energy expression, the strain energy expression is quadratic with respect to the control voltage vector:

$$\overline{U}_{\text{bending}} = \mathbf{V}_{\text{con}}^{\text{H}} \mathbf{SE}_Q \mathbf{V}_{\text{con}} + \mathbf{SE}_S^{\text{H}} \mathbf{V}_{\text{con}} + \mathbf{V}_{\text{con}}^{\text{H}} \mathbf{SE}_T + \text{SE}_P. \tag{21}$$

The primary goal is to find the control voltage that yields maximum loss factor. The first step in determining the critical voltage is to take a first variation of the total loss factor of the ACLD with respect to the control voltage. This generates the following condition that can be used to compute the control voltage:

$$\frac{\partial \eta^{\text{Tot}}}{\partial \mathbf{V}_{\text{con}}^*} = 0 \Rightarrow \overline{U}_{\text{bending}} \frac{\partial \sum_{k=1}^{\#\text{ACLD}} \Delta \overline{W}_d^k}{\partial \mathbf{V}_{\text{con}}^*} - \sum_{k=1}^{\#\text{ACLD}} \Delta \overline{W}_d^k \frac{\partial \overline{U}_{\text{bending}}}{\partial \mathbf{V}_{\text{con}}^*} = 0. \tag{22}$$

This is the numerator of the resulting expression after applying the quotient rule. By substituting Eqs. (19) and (21) into Eq. (22), it becomes a system of coupled, complex cubic polynomial equations with the control voltage vector as the independent variable that must be solved iteratively. When there is only one ACLD, however, the system of complex cubic equations reduces to a scalar second order complex polynomial equation. In the subsequent analysis, only the single ACLD case is going to be considered. Because of this, all the indices in the subsequent mathematical expressions are dropped for convenience. The resulting second-order polynomial equation for single ACLD case is

$$\begin{aligned} &V_{\text{con}}^2 \left[\text{SE}_S \text{DE}_Q - \text{DE}_S \text{SE}_Q\right] \\ &\quad + V_{\text{con}} \left[\text{SE}_P \text{DE}_Q + \text{SE}_S \text{DE}_T - \text{DE}_P \text{SE}_Q - \text{DE}_S \text{SE}_T\right] \\ &\quad + \left[\text{SE}_P \text{DE}_T - \text{DE}_P \text{SE}_T\right] = 0. \end{aligned} \tag{23}$$

The V_{con} is solved by applying the quadratic equation. The computed V_{con} ensures that the loss factor reaches a critical value with respect to control voltage. In order to ensure that the loss factor with the control voltage reaches a maximum, twice-differentiated Eq. (20) with the critical V_{con} must result in a negative value. Due to the complex nature of the coefficients, a result of differentiation in an equation form does not provide any definite conclusion of the critical nature of the resulting loss factor. The subsequent numerical analysis demonstrates that the computed critical control voltage causes the loss factor to become a maximum at resonant frequency bands of the structure. This is discussed in detail in the next section.

3. Results and discussions

3.1. Validation of the active constrained layer damping model

The mathematical modeling approach of the ACLD system is validated by comparing it with an experimental result previously reported by Liao and Wang [21]. The compared experimental result shows the tip displacement of a cantilever beam excited by the ACLD. Tables 1 and 2 [21] lists the physical and material specifications of the structural system used in the validation phase. Fig. 3 shows a diagram showing a general layout of the system. The tested structural system consists of a cantilevered aluminum beam with a bonded ACLD, which covers approximately 40% of beam's length. The active constrained layer is made of a PZT ceramic (PKI 502). The input voltage to the constrained layer is a white noise signal. A fiber optic displacement sensor is placed at the free end of the beam to measure its tip displacement. Eqs. (24a–d) describe the frequency-dependent shear storage modulus and its loss factor of the viscoelastic material (3M IDS 112) [21]. Fig. 4 shows the frequency variant store and loss (real and imaginary) moduli of the viscoelastic layer:

$$G(\omega) = G(\omega)' + \mathrm{j}G(\omega''), \tag{24a}$$

Table 1
Parameters of the validated system [21]

Beam length: a (m)	0.261	PZT thickness: h_c (m)	0.000762	α	6.0
Beam width: b (m)	0.0127	PZT piezoelectric constant: $d31_c$ (m/V)	$-175E$–12	κ (N/m^2)	5E5
Beam thickness: h_b (m)	0.002286	PZT Young's modulus: $Q11_c$ (N/m^2)	7.4E10	$\hat{\varsigma}$	4.0
Beam's Young's modulus: $Q11_b$ (N/m^2)	7.1E10	Viscoelastic layer thickness: h_v (m)	0.00025	$\hat{\omega}$ (rad)	10000
Beam density: ρ_b (kg/m^3)	2700	PZT density: ρ_c (kg/m^3)	7600	Viscoelastic material density: ρ_v (kg/m^3)	1250

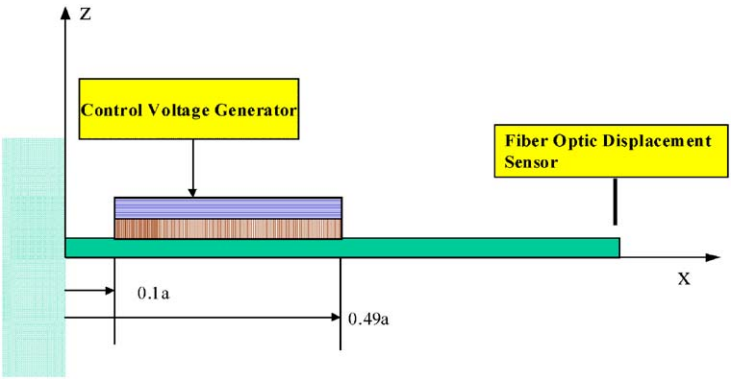

Fig. 3. Diagram of the validated system.

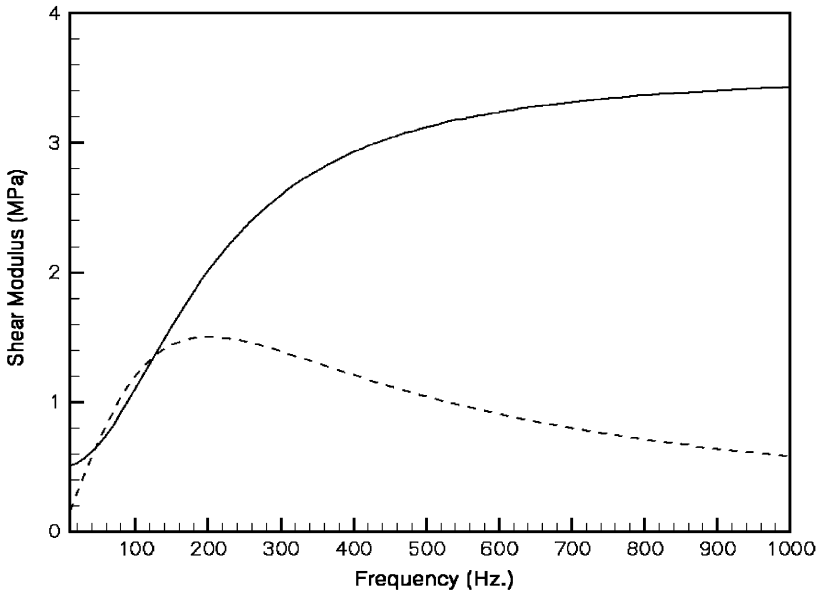

Fig. 4. Frequency-dependent properties of the shear moduli of the viscoelastic material 3M IDS 112: ——, stored modulus; - - - -, loss modulus.

$$G(\omega)' = \kappa\left[1 + \alpha\frac{\omega^4 + (4\hat{\varsigma}^2 - 1)\hat{\omega}^2\omega^2}{\omega^4 + 2(2\hat{\varsigma}^2 - 1)\hat{\omega}^2\omega^2 + \hat{\omega}^4}\right], \tag{24b}$$

$$\eta(\omega) = \alpha\left[\frac{2\hat{\varsigma}\hat{\omega}^3\omega}{(1+\alpha)\omega^4 + (4(1+\alpha)\hat{\varsigma}^2 - 1)\hat{\omega}^2\omega^2 + \hat{\omega}^4}\right], \tag{24c}$$

$$G(\omega)'' = G(\omega)'\eta(\omega). \tag{24d}$$

Fig. 5 shows a comparison between the predicted and experimentally measured tip displacements of the beam normalized by the input voltage signal. It illustrates that the experimental and analytical results are in a good agreement. The first and the second modes predicted by the analytical model are at 25.25 and 151 Hz, respectively. The experimental result shows that the modal frequencies are at 26.5 and 148.75 Hz. The percentage differences between the results for the first and the second modes are 4.7% and 1.5%, respectively. For the beams with different boundary conditions, the only variation in the model is different mode shape functions. Therefore, this validation conclusively proves that the general formulation of the ACLD model is accurate.

3.2. *Performance of active constrained layer damping treatment*

The beam and the ACLD used in the validation phase are utilized in the subsequent analysis. The applied boundary conditions of the beam are the those previously discussed in the Theory Section. All 3 beams have one ACLD. For the simply supported and clamped boundary condition

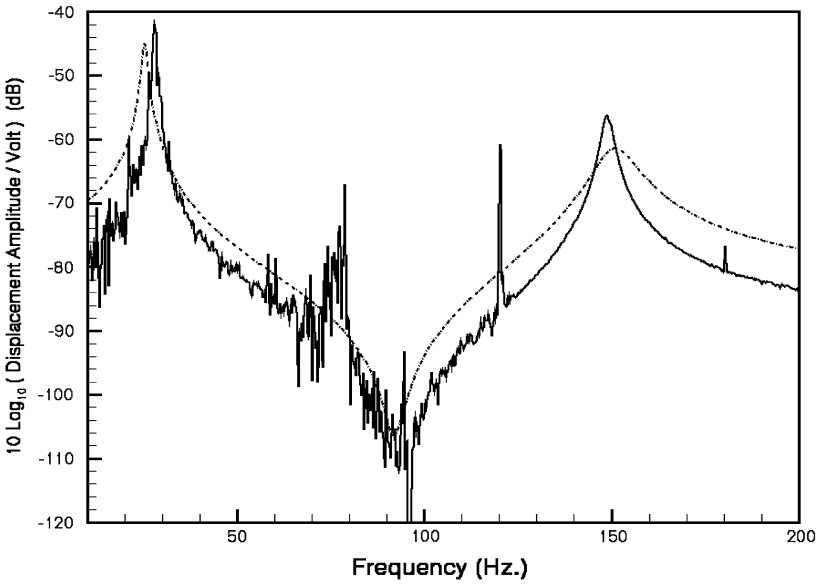

Fig. 5. Tip displacement comparison between the analytical and experimental results: - - - -, analytical; ——, experimental.

cases, the segment of the beam with the ACLD is from $\xi = 0.3$ to 0.7. For the cantilevered beam, the same coverage used in the validation case is applied. This location is near the clamped end of the beam where a high level of strain is exhibited. A constant pressure load of 1 Pa with uniform phase is applied to the beam as a primary disturbance excitation. This is equivalent to a constant 94 dB plane wave acoustic excitation spectra.

3.2.1. *Maximization of loss factor*

The critical control voltage is computed applying the quadratic equation to Eq. (23). Of the two answers, the one with smaller amplitude is used. Figs. 6–8 show the computed V_{con}. The figures reveal 3 distinctive phases in transformation of the control voltage near natural frequencies of the beams. As the excitation frequency approaches natural frequencies of the beams, the voltages show a typical frequency response of rapid, smooth increase. As the frequency reaches a resonant frequency, the voltages suddenly shift to a linearly decreasing pattern. This pattern holds until the frequency passes beyond the resonant frequency. Then, the voltages reverse back to a typical frequency response pattern of decay.

From the figures, three trends can be observed. First, the peak control voltage amplitude decreases as frequency increases. For example, for the simply supported beam case, the voltage remains in a linearly decreasing pattern from 7.19 V at 74 Hz to 6.45 V at 84 Hz for the first mode. For the third mode, the control voltage changes from 0.16 V at 650 Hz to 0.159 V at 754 Hz. The average control voltage amplitude for the first mode is 6.82 V, while it is dropped to 0.1595 V for the third mode. Second, the frequency bandwidth of the peak voltage region increases as the frequency increases. The frequency bandwidths for the first and third modes are 10 and 104 Hz, respectively. Third, the rate of decrease in

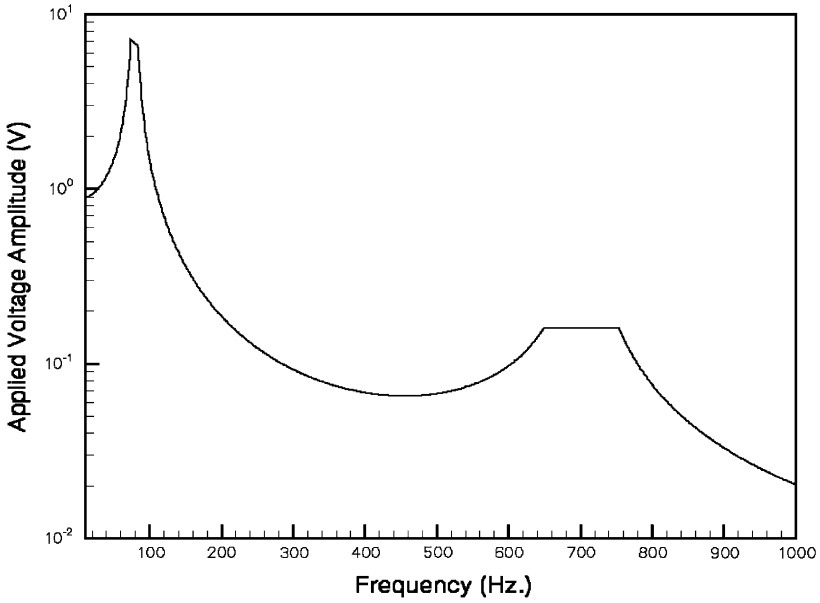

Fig. 6. Amplitudes of the applied voltage and the electric field of the ACLD from a first variation of the overall loss factor with respect to the control voltage for the simply supported beam.

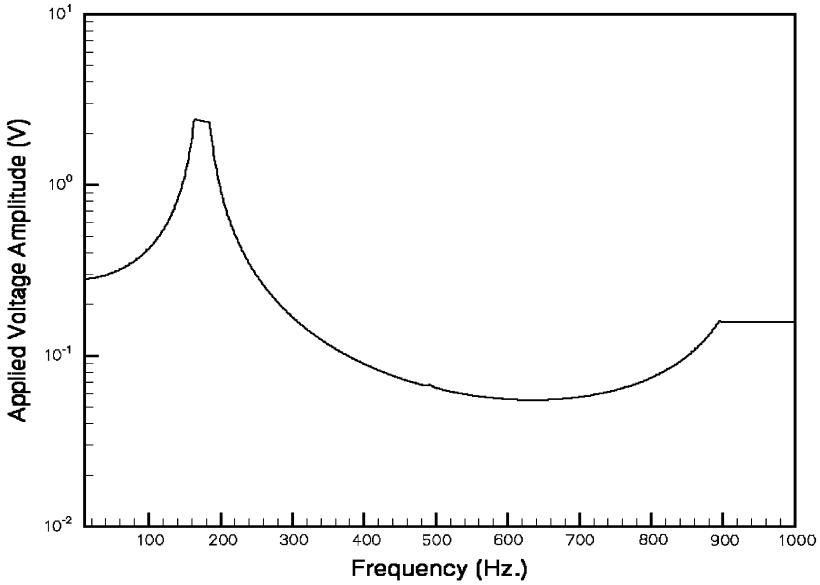

Fig. 7. Amplitudes of the applied voltage and the electric field of the ACLD from a first variation of the overall loss factor with respect to the control voltage for the clamped beam.

the peak voltage within the resonant frequency band decreases as frequency increases. The rates of decrease in the voltage within the resonant frequency band of the first and third modes are 0.074 and 9.6 μV/Hz, respectively. Therefore, the frequency bandwidth and the change in the

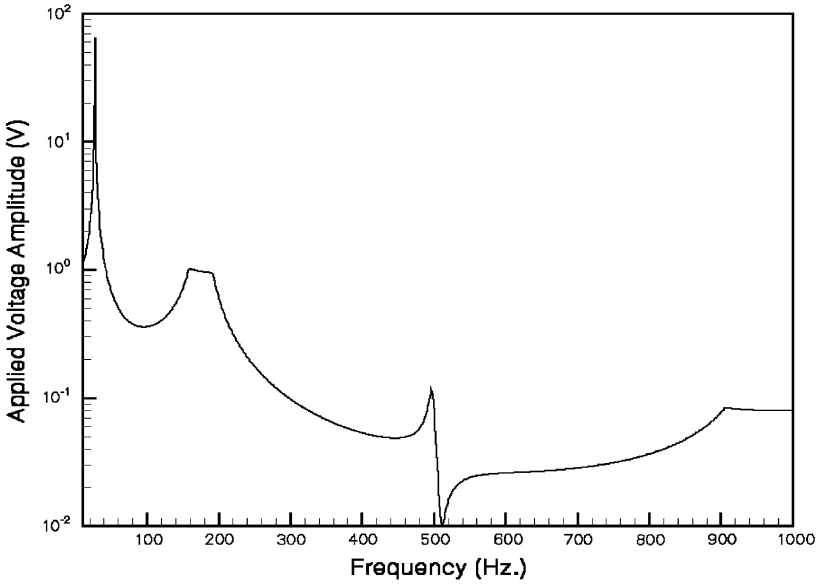

Fig. 8. Amplitudes of the applied voltage and the electric field of the ACLD from a first variation of the overall loss factor with respect to the control voltage for the cantilevered beam.

computed peak control voltage within resonant frequency ranges show an inversely proportional relationship.

Unlike either the simply supported or clamped beams, the control voltage for the cantilevered beam shows a slightly different pattern, as shown in Fig. 8. Although it shows the linear patterns around the resonant frequencies, the corresponding frequency bandwidths are significantly narrower than the other beams. Also, the voltage shows a resonant–anti resonant pattern, instead of the linear pattern, at the third mode. In the same context, neither the simply supported nor the clamped beam show any change in the control voltage at their second modes.

With the critical control voltages, the corresponding loss factors are computed using Eq. (20). Figs. 9–11 show the comparisons between the overall (active + passive) and passive loss factors of the beams. By applying the critical voltages, the loss factors become significantly lower than their passive counterparts in off-resonant frequency ranges. However, in the resonant frequency band of the beams, the overall loss factors become significantly greater than the passive factors. Recalling that the voltage is computed by differentiating the loss factor expression with respect to the control voltage, this trend suggests that the critical control voltage makes the performance of the ACLD maximum where the damping effect becomes dominant.

The frequency bandwidths of the active loss factors around the natural frequencies of the beams show the identical trends as the control voltage. When the control voltages abruptly switch to the linear patterns, the corresponding loss factors are "switched on" and become maximum. Once the control voltages switch back to smooth decaying patterns, then the loss factors become "switched off" and return to their minimum states. For the cantilevered beam, in addition to the patterns discussed, both the active and passive loss factors reach the same level at the third mode. This is where the voltage shows a resonant–anti-resonant pattern in Fig. 8.

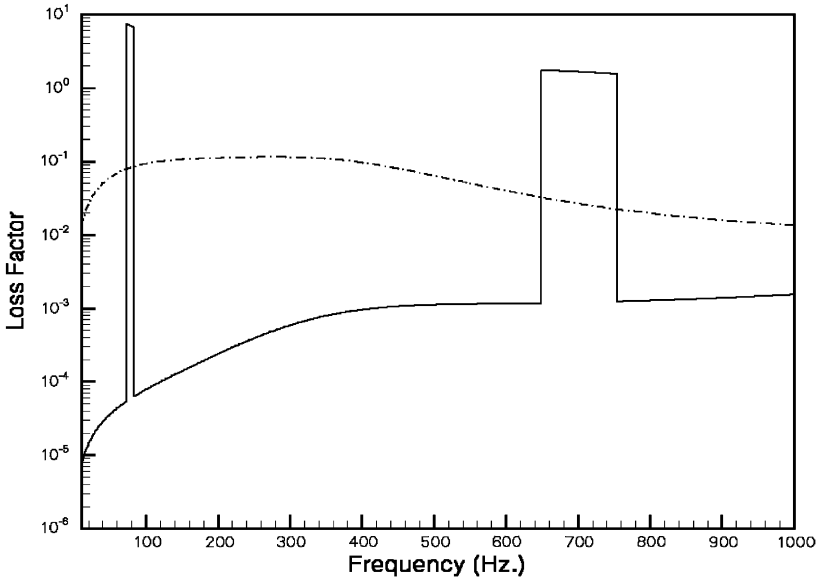

Fig. 9. Loss factor comparison between a passive and an active ACLD for the simply supported beam: ——, active; - - - - -, passive.

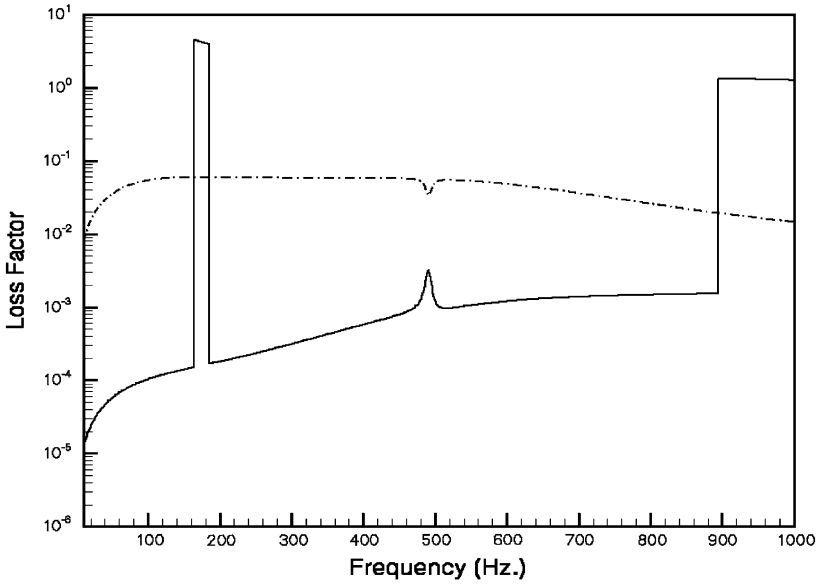

Fig. 10. Loss factor comparison between a passive and an active ACLD for the clamped beam: ——, active; - - - - -, passive.

To verify the nature of criticality of the control voltage, the loss factors are differentiated twice with respect to the control voltage. Fig. 12 shows the real components of the results. Compared to the real component, the imaginary component of the twice-differentiated loss factors are

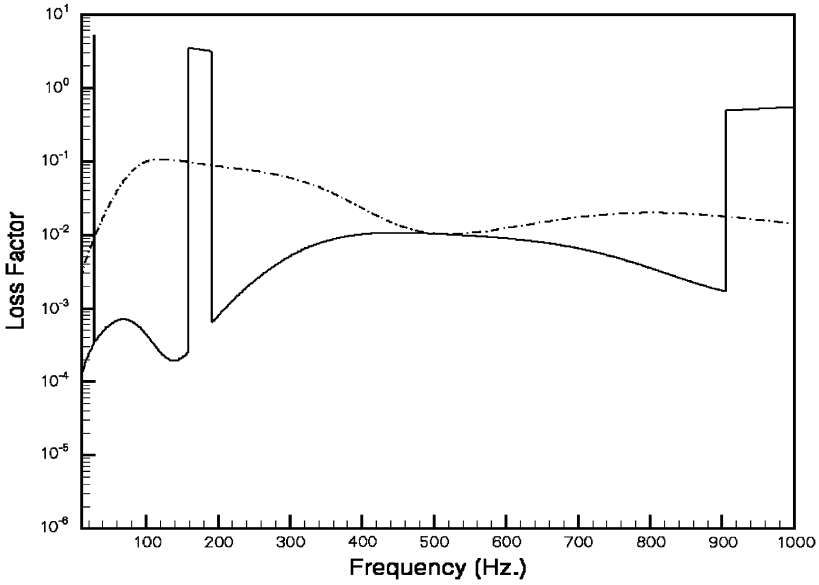

Fig. 11. Loss factor comparison between a passive and an active ACLD for the cantilevered beam: ——, active; - - - -, passive.

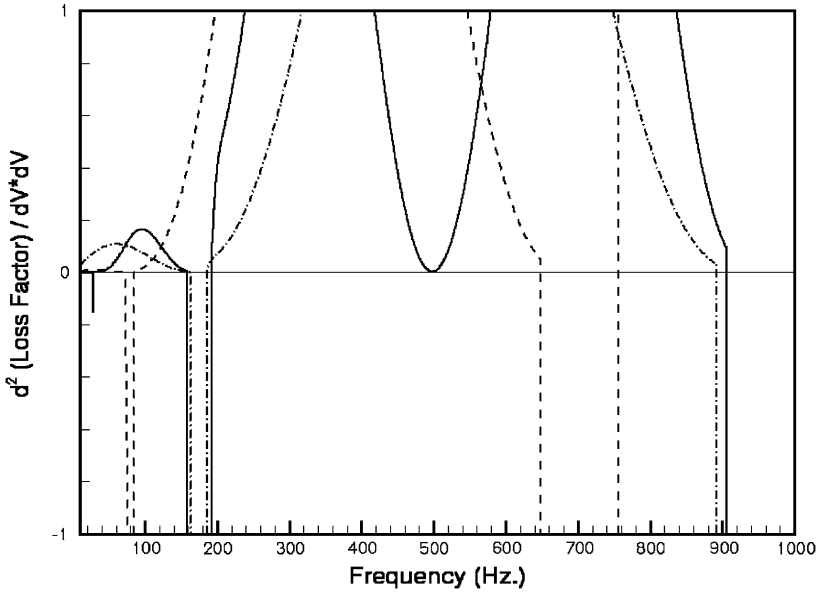

Fig. 12. Real component of $\partial^2 \eta_{TOT}/\partial V^*_{con} \partial V_{con}$ for the simply supported beam: ——, cantilevered; - - - -, clamped; - - - -, simply supported.

determined to be noninfluential in the criticality. As the figures indicate, the twice-differentiated loss factors increase as a frequency approaches natural frequencies. Then, they shift the phase to negative. After passing the natural frequencies, they switch back to positive again. This sudden

shift in phase of the twice-differentiated loss factor causes the loss factors to switch abruptly from the minimum to maximum states.

The resulting control voltage turns the ACLD into a highly effective energy dissipating device. A damping effect becomes dominant only at resonant frequency zones of a structure. Because the control voltage is determined through differentiating the loss factor expression, it causes the resulting critical loss factor to reach local maximum only at resonant frequency zones. Due to this consideration, Eq. (22) can be regarded as a condition for an ACLD in maximizing its energy dissipating capability.

3.2.2. *Performance of the ACLD with the critical loss factors*

The next stage is to investigate the effect of the control voltage on structural dynamic responses by observing two physical quantities; kinetic energy of the host beams and resulting average far-field radiated sound power. Kinetic energy is a useful quantity in evaluating the overall dynamic behavior of a vibrating structure. It not only reveals its dynamic behavior, the energy also indicates the level of radiated sound power in the near field [28]. The kinetic energy due to flexural motion of the beams is observed in evaluating the effectiveness of the ACLD.

3.2.2.1. Reduction in kinetic energy. From observing the reduction of kinetic energies of the beams in Figs. 13–15, the significant reduction in vibratory energy by ACLD is evident. For the lower order modes, the reduction level is high and the effective frequency bandwidth narrow. As the frequency increases, the reduction level decreases but the effective frequency bandwidth increases significantly. For example, reductions in kinetic energy for the simply supported beam by the ACLD are 61 dB for the first mode and 35 dB for the third mode.

This inversely proportional pattern between the kinetic energy and the associated resonant frequency bandwidth correlates to the trend of the loss factors and the control voltages shown earlier. This may be contributed to the two factors. First, as the excitation frequency increases, the resonant vibration amplitude goes down. This translates into a decreasing trend in reduction in the kinetic energy by the ACLD. Second, the overall effectiveness of a viscoelastic constrained layer damping treatment increases as the frequency goes up. Therefore, the effective control frequency bandwidth of the ACLD increases accordingly.

Another noticeable trend is that the kinetic energy is significantly reduced by the passive ACLD alone. This indicates that the ACLDs are placed in effective locations to dissipate the vibration energy of the beams. Therefore, this strongly suggests that the maximization of the loss factor is also dependent on location of the ACLD.

3.2.2.2. Reduction in radiated sound power. The radiated sound power of the beams is computed using Eqs. (25) [29]. One key assumption applied to the cantilevered beam is that the free end is acoustically sealed.

$$\Pi = \int_{\varphi=0}^{\varphi=2\pi} \int_{\theta=0}^{\theta=\pi/2} \frac{|P|^2}{2\rho_{\text{air}} c} r^2 \sin\theta \, \mathrm{d}\theta \, \mathrm{d}\varphi = \int_{\varphi=0}^{\varphi=2\pi} \int_{\theta=0}^{\theta=\pi/2} I r^2 \sin\theta \, \mathrm{d}\theta \, \mathrm{d}\varphi, \tag{25a}$$

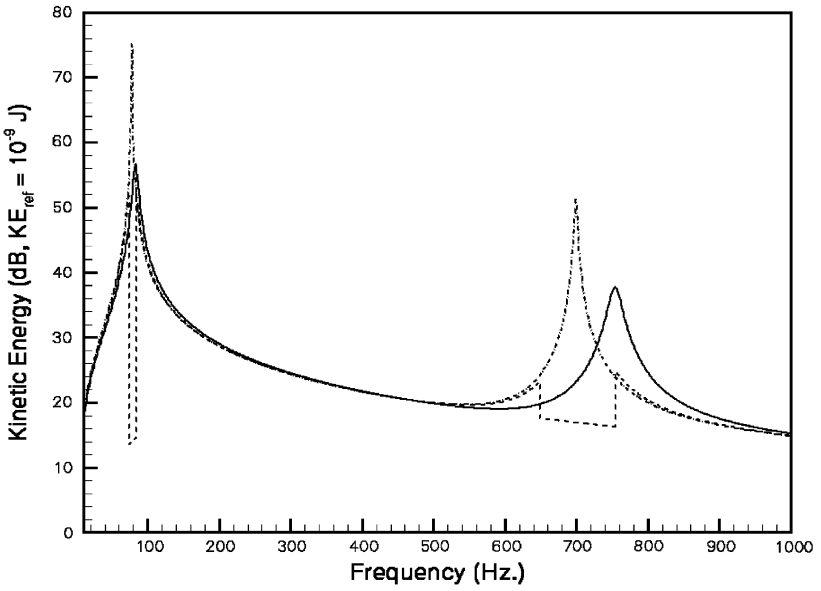

Fig. 13. Reduction in the kinetic energy of simply supported beam by the damping treatments: - · - · -, no damping; ——, passive damping; - - - -, active damping.

where

$$P = \mathrm{j}\omega\rho_{\mathrm{air}}\frac{\mathrm{e}^{-\mathrm{j}kr}}{2\pi r}\int_A \frac{\partial w}{\partial t}\,\mathrm{e}^{\mathrm{j}\alpha x/a}\mathrm{e}^{\mathrm{j}\beta y/b}\,\mathrm{d}y\,\mathrm{d}x. \tag{25b}$$

The average far-field sound powers radiated by the 3 beams are shown in Figs. 16–18. As shown in the kinetic energy reduction, the sudden changes in the loss factors affect the sound power as well. For the first mode, the maximization of the loss factors causes the sound power to be dramatically reduced to below 0 dB for all the beams. For the higher modes, the resonant peaks are dropped to nonresonant levels. This demonstrates that the ACLD is effective in controlling the structural acoustic response of the beams.

4. Conclusions

This research investigates the application of active constrained layer damping treatment to control dynamic responses of beams with classic boundary conditions. Generally, a passive viscoelastic damping treatment is effective for high-frequency vibrations. In the low- to mid-frequency ranges, the treatment becomes ineffective because of the greater wavelength of the vibrating structure compared to the damping treatment coverage length. This research has demonstrated that an active constrained layer damping treatment can effectively damp out low-frequency vibrations as well.

The control voltage that maximizes the loss factor can significantly reduce the vibrations and noise of the beams at the resonant frequencies. Because the control voltage is determined through the first variation of the loss factor with respect to the voltage, it is demonstrated that the resulting

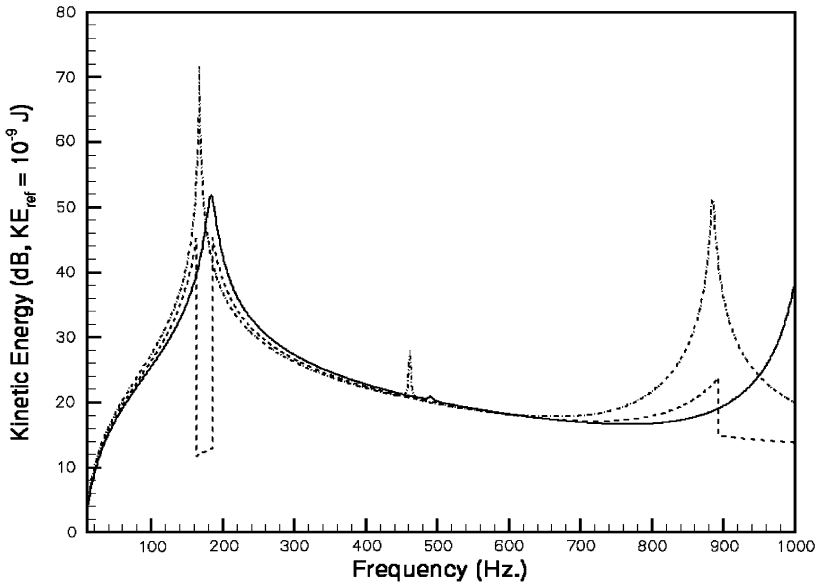

Fig. 14. Reduction in the kinetic energy of clamped beam by the damping treatments: - · · · -, no damping; ——, passive damping; - - - -, active damping.

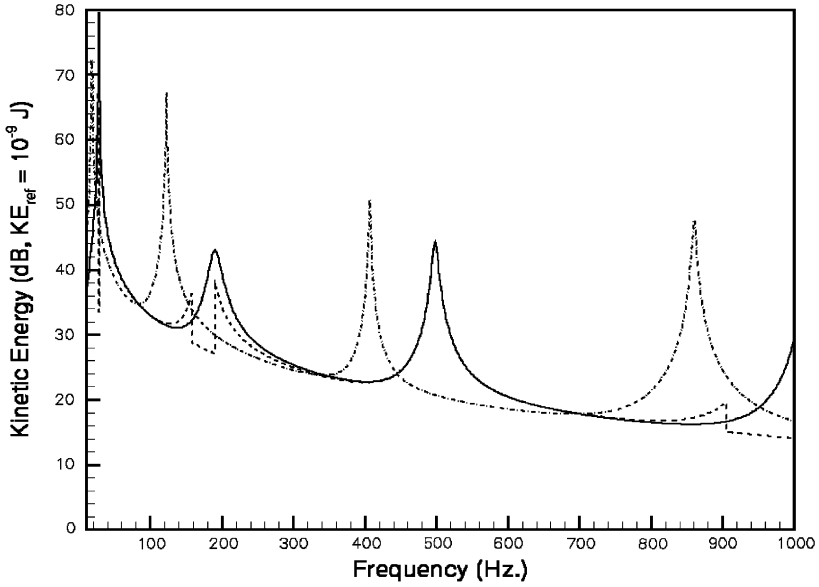

Fig. 15. Reduction in the kinetic energy of cantilevered beam by the damping treatments: - · · · -, no damping; ——, passive damping; - - - -, active damping.

loss factor has to be maximum in the resonant frequency and minimum in the off-resonant frequency bands. Its nature of criticality is illustrated through the double differentiation of the loss factor with respect to the voltage.

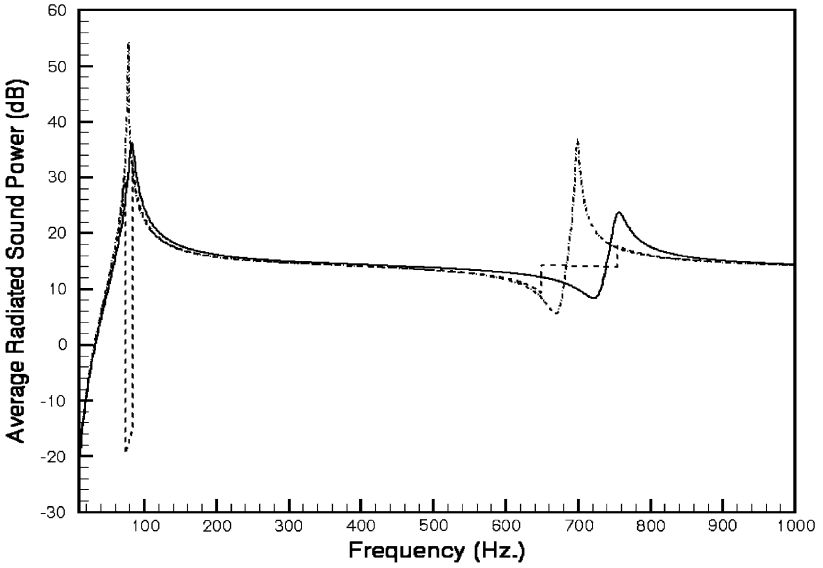

Fig. 16. Reduction in the radiated sound power of the simply supported beam by the damping treatments: - · - · -, no damping; ——, passive damping; - - - -, active damping.

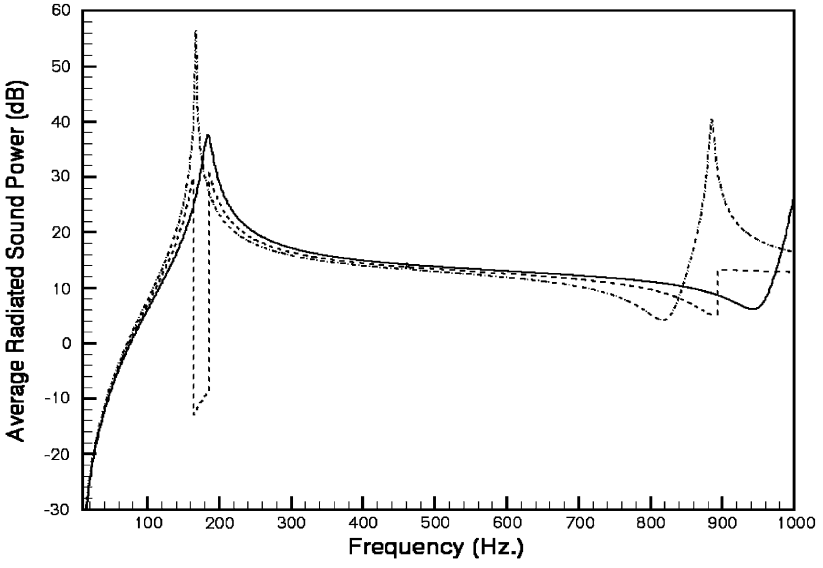

Fig. 17. Reduction in the radiated sound power of the clamped beam by the damping treatments: - · - · -, no damping; ——, passive damping; - - - -, active damping.

Although this research has demonstrated the potential of the ACLD, there are many issues that must be resolved. The control voltage is determined with the knowledge of the full state of the beams and the constrained layer damping. Consequently, this is the best performance that the

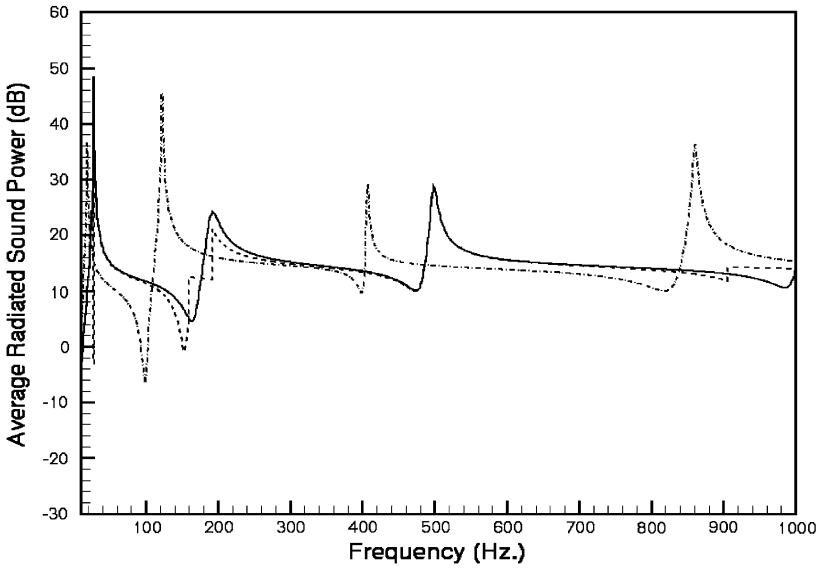

Fig. 18. Reduction in the radiated sound power of the cantilevered beam by the damping treatments: - · - · -, no damping; ——, passive damping; - - - -, active damping.

ACLD can promise. If the voltage is determined through utilizing partial information of the system, then it is clear that the same level of performance of the ACLD cannot be guaranteed. Also, a control scheme that can implement the loss factor-maximizing the control voltage must be developed. Resolution of these issues ensures the robustness of the ACLD and, thus, paves a way to make it a viable mean to control the vibration and sound of structural systems.

Acknowledgement

The author would like to thank Professor W.H. Liao of The Chinese University of Hong Kong for generously providing the experimental data used in the validation of the analytical model.

Appendix A. Applied mode shapes

A.1. Longitudinal displacement field of kth active constrained layer

$$u_c^k(x, x_o^k, t, \omega) = \left(C^k + \sum_{n=1}^{N3} U_c^k(n) Q(k, n, x) \right)$$
$$= \left(C^k + \sum_{n=1}^{N3} U_c^k(nc) \cos\left(\frac{n\pi(x - x_o^k)}{a} \right) \right) e^{j\omega t}, \quad n = 1, 2, 3, ..., N3.$$

Table 2
Eigenfunction parameters for cantilevered and clamped beams [27]

Boundary conditions	Cantilevered		Clamped	
Mode number (m)	k_m	R_m	k_m	R_m
1	0.7340955	1.8751041	0.9825022	4.7300408
2	1.0184664	4.6940911	1.0007773	7.8532046
3	0.9992245	7.8547574	0.9999665	10.9956078
4	1.0000336	10.995541	1.0000015	14.1371655
5	0.9999986	14.137168	0.9999999	17.2787596
6	1.0	17.278745	1.0	20.4203522
$m>6$	1.0	$(2m-1)\pi/2$	1.0	$(2m+1)\pi/2$

A.2. Transverse displacement field of the beam

Boundary condition: simply supported.

$$w(x,t,\omega)=\sum_{m=1}^{N5}\sin\left(\frac{m\pi x}{a}\right)e^{j\omega t},\quad m=1,2,3,\ldots,N5.$$

Boundary condition: clamped on both ends or cantilevered.

$$w(x,t,\omega)=\sum_{m=1}^{N5}\left[\cosh\left(k_m\frac{x}{a}\right)-\cos\left(k_m\frac{x}{a}\right)-R_m\left(\sinh\left(k_m\frac{x}{a}\right)-\sin\left(k_m\frac{x}{a}\right)\right)\right]e^{j\omega t}.$$

References

[1] D.J. Mead, S. Markus, The forced vibration of a three-layer, damped sandwich beam with arbitrary boundary conditions, *Journal of Sound and Vibration* 10 (1969) 163–175.
[2] R. Plunkett, C.T. Lee, Length optimization for constrained viscoelastic layer damping, *Journal of Acoustical Society of America* 48 (1970) 150–161.
[3] Y.P. Lu, J.C. Clemens, A.J. Roscoe, Vibrations of composite plate structures consisting of a constrained-layer damping sandwich with viscoelastic core, *Journal of Sound and Vibration* 158 (1992) 552–558.
[4] Y.V.K. Sadasiva Rao, B.C. Nakra, Vibrations of unsymmetrical sandwich beams and plates with viscoelastic cores, *Journal of Sound and Vibration* 34 (1974) 309–326.
[5] C.T. Sun, Y.P. Lu, *Vibration Damping of Structural Elements*, Prentice-Hall, Englewood Cliffs, NJ, 1995.
[6] A.D. Nashif, D.I.G. Jones, J.P. Henderson, *Vibration Damping*, Wiley, New York, 1985.
[7] A.K. Lall, N.T. Asnani, B.C. Nakra, Damping analysis of partially covered sandwich beams, *Journal of Sound and Vibration* 123 (1988) 247–259.
[8] A.K. Lall, N.T. Asnani, B.C. Nakra, Vibration and damping analysis of rectangular plate with partially covered constrained viscoelastic layer, *ASME Journal of Vibration, Acoustics, Stress, and Reliability in Design* 109 (1987) 241–247.
[9] S.-W. Kung, R. Singh, Vibration analysis of beams with multiple constrained layer damping patches, *Journal of Sound and vibration* 212 (1998) 781–805.

[10] S.-W. Kung, R. Singh, Complex eigensolutions of rectangular plates with damping patches, *Journal of Sound and Vibration* 216 (1998) 1–28.
[11] P. Trompette, D. Boillot, M.A. Ravanel, The effect of boundary conditions on the vibration of a viscoelastically damped cantilever beam, *Journal of Sound and Vibration* 60 (1978) 345–350.
[12] C.H. Park, A. Baz, Vibration control of bending modes of plates using active constrained layer damping, *Journal of Sound and Vibration* 227 (1999) 711–734.
[13] M.C. Ray, A. Baz, Optimization of energy dissipation of active constrained layer damping treatments of plates, *Journal of Sound and Vibration* 208 (1997) 391–406.
[14] A. Baz, Optimization of energy dissipation characteristics of active constrained layer damping, *Smart Material and Structure* 6 (1997) 360–368.
[15] A. Baz, Boundary control of beams using active constrained layer damping, *ASME Journal of Vibration and Acoustics* 119 (1997) 166–172.
[16] I.Y. Shen, A variational formulation, a work-energy relation and damping mechanisms of active constrained layer treatments, *ASME Journal of Vibration and Acoustics* 119 (1997) 192–199.
[17] C. Chantalakhana, R. Stanway, Active constrained layer damping of clamped–clamped plate vibrations, *Journal of Sound and Vibration* 241 (2001) 755–777.
[18] Y.M. Shi, Z.F. Li, H.X. Hua, Z.F. Fu, T.X. Liu, The modeling and vibration control of beams with active constrained layer damping, *Journal of Sound and Vibration* 245 (2001) 785–800.
[19] V. Balamurugan, S. Narayanan, Finite element formulation and active vibration control study on beams using smart constrained layer damping (SCLD) treatment, *Journal of Sound and Vibration* 249 (2002) 227–250.
[20] D.H. Kruger, J.A. Mann III, T. Wiegandt, Placing constrained layer damping patches using reactive shearing structural intensity measurements, *Journal of Acoustical Society of America* 101 (1997) 2075–2082.
[21] W.H. Liao, K.W. Wang, On the analysis of viscoelastic materials for active constrained layer damping treatments, *Journal of Sound and Vibration* 207 (1997) 319–334.
[22] W.H. Liao, K.W. Wang, On the active–passive hybrid control actions of structures with active constrained layer treatments, *ASME Journal of Vibration and Acoustics* 119 (1997) 563–572.
[23] Y. Liu, K.W. Wang, Damping optimization by integrating enhanced active constrained layer and active–passive hybrid constrained layer treatments, *Journal of Sound and Vibration* 255 (2002) 763–775.
[24] Y. Liu, K.W. Wang, A non-dimensional parametric study of enhanced active constrained layer damping treatments, *Journal of Sound and Vibration* 223 (1999) 611–644.
[25] J.A. Rongong, J.R. Wright, R.J. Wynne, G.R. Tomlinson, Modelling of a hybrid constrained layer/piezoceramic approach to active damping, *ASME Journal of Vibration and Acoustics* 119 (1997) 120–130.
[26] M.J. Lam, D.J. Inman, W.R. Saunders, Vibration control through passive constrained layer damping and active control, *Journal of Intelligent Material Systems and Structures* 8 (1997) 663–677.
[27] A. Leissa, Vibration of plates, NASA SP-160, 1969, N70-18461.
[28] S.J. Elliott, P. Gardonio, T.C. Sors, M.J. Brennan, Active vibroacoustic control with multiple local feedback loops, *Journal of Acoustical Society of America* 111 (2002) 908–915.
[29] K. Cunefare, The minimum multimodal radiation efficiency of baffled finite beams, *Journal of Acoustical Society of America* 90 (1991) 2521–2529.
[30] J.T. Lee, Active structural acoustic control using active constrained layer damping system and secondary acoustic controller, Ph.D. Thesis, University of California, Los Angeles, 2003.